Nanoscale

Accepted Manuscript

This article can be cited before page numbers have been issued, to do this please use: L. Hu, X. Tian, Y. Huang, L. Fang and Y. Fang, *Nanoscale*, 2016, DOI: 10.1039/C5NR08527F.

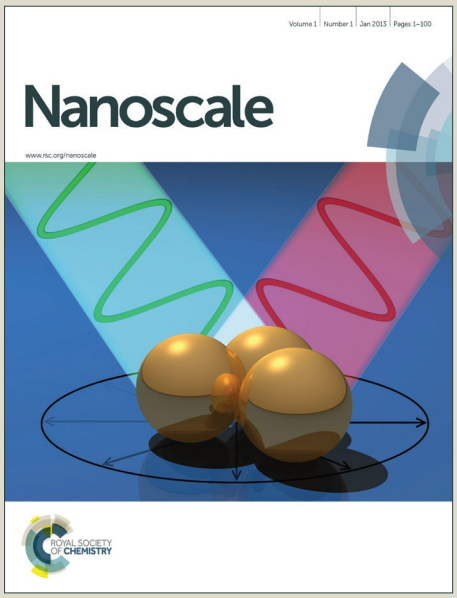

ROYAL SOCIETY OF CHEMISTRY

www.rsc.org/nanoscale

View Article Online
DOI: 10.1039/C5NR08527F

Quantitatively analyzing the mechanism of giant circular dichroism in extrinsic plasmonic chiral nanostructures by tracking the interplay of electric and magnetic dipoles

Li Hu[1,4,†], Xiaorui Tian[2,†], Yingzhou Huang[1], Liang Fang[1] and Yurui Fang[3,*]

[1]Soft Matter and Interdisciplinary Research Center, College of Physics, Chongqing University, Chongqing, 400044, P. R. China

[2]College of Chemistry, Chemical Engineering and Materials Science, Shandong Normal University, Jinan 250014, China

[3]Bionanophotonics, Department of Applied Physics, Chalmers University of Technology, Göteborg, SE-41296, Sweden

[4]School of Computer Science and Information Engineering, Chongqing Technology and Business University, Chongqing, 400067, China

†These authors contributed equally

*Corresponding Email: yurui.fang@chalmers.se (Y. Fang)

Abstract

Plasmonic chirality has drawn much attention because of tunable circular dichroism (CD) and the enhancement of chiral molecule signals. Although various mechanisms have been proposed to explain the plasmonic CD, a quantitative explanation like the ab initio mechanism for chiral molecules, is still unavailable. In this study, a mechanism similar to the mechanisms associated with chiral molecules was analyzed. The giant extrinsic circular dichroism of a plasmonic splitting rectangle ring was quantitatively investigated from a theoretical standpoint. The interplay of the electric and magnetic modes of the meta-structure is proposed to explain the giant CD. We analyzed the interplay using both an analytical coupled electric-magnetic dipoles model and a finite element method model. The surface charge distributions showed that the circular current yielded by the splitting rectangle ring causes the ring to behave like a magneton at some resonant modes, which then interact with electric modes, resulting in a mixing of the two types of modes. The strong interplay of the two mode types is primarily responsible for the giant CD. The analysis of the chiral near-field of the structure shows potential applications for chiral molecule sensing.

Keywords: circular dichroism, surface plasmon, plasmonic chirality, magnetic mode, meta-molecule

Introduction

The optical chirality due to different responses of the handedness or asymmetry of an object to the spin of light is very weak, but it is very important in nature.[1] The analysis of chiral effects is of significance in the study of medical diagnostics, crystallography, analytical chemistry, molecular biology and life forms

View Article Online
DOI: 10.1039/C5NR08527F

in the universe.[2] However, the weak chiral response of natural molecules has limited their applications, especially when the target in question is tiny. One recent way is designing metal nanostructures to enhance or yield such effects, in which surface plasmons (SPs), the collective oscillation of free electrons, play key roles. Surface plasmon resonance is sensitively dependent on the shape, size, material, as well as the configuration of nanostructures, allowing them to be flexibly manipulated and applied in various areas.[3] Metal nanostructures have been considered as good candidates for associating the chiral effect and extending the existence of chirality in nature.[4-6]

The optical activity of plasmonic nanostructures has attracted increasing attention as an emerging area in recent years. Optical activities such as optical rotatory dispersion (ORD) and circular dichroism (CD) are produced by the mirror asymmetry (chirality) of structures. A pure two-dimensional asymmetric structure under normal excitation incidence is thought to only have birefringence effects, which only yield ORD. While chiral structures that are able to yield CD should be three-dimensional, at least in some way (e.g., substrate image effect)[7], so that their mirror forms cannot be superimposed with themselves through a sequence of rotations and translations.[1] Over the past several years, various chiral plasmonic nanostructures have been investigated for their optical activities, such as chiral metal particles,[8, 9] pairs of mutually twisted planar metal patterns,[10] single-layered metal sawtooth gratings,[11] planar chiral metal patterns,[12] DNA-based self-assembled metal particles,[13, 14] and metal helices.[15-17] For a straightforward geometric definition, chirality can be obtained from achiral nanostructures simply by tilting their symmetry axis out of the incident plane to yield a three-dimensional asymmetry, which is so-called extrinsic chirality.[18-20] Giant circular dichroism has been obtained with these extrinsic chiral structures since 2009.[18] Extrinsic chirality not only provides a more flexible way to overcome the difficulty of the fabrication progress associated with complex chiral structures but also shows even stronger CD than the intrinsic one. A near 100% difference of the response to spin light was theoretically predicted last year for the extrinsic chirality of plasmonic nanorice heterodimers due to the Fano-associated effect.[21]

Several explanations have been proposed for the generation of CD effect of plasmonic chiral structures, such as the phase delay for the two orthogonal directions of structures, the asymmetry of a structure to circularly polarized light (CPL), the resonant modes that overlap the rotational direction of the CPL, and so on. However, they are basically phenomenological and qualitative. The phase change is mostly addressed in a qualitative fashion. A more general, profound approach is analogous to the plasmonic structure as a chiral molecule, the chiral mechanism of which has been well investigated and explained using ab initio theory. In the chiral molecule model, the chiral mechanism obtained with the ab initio model is such that the chiral effect comes from the interaction of the electric and magnetic dipoles.[1] This idea was borrowed by Plum[18, 19] to explain the extrinsic chirality of plasmonic structures qualitatively. Later, Tang[22] borrowed from Lipkin's theory[23] and addressed the chirality of the chiral field. The chirality of plasmonic structures and the chirality enhancement of plasmonic structures can be explained by combining these two ideas.[21, 24-26] However, an analytical or quantitative explanation of the CD is still unavailable.

In this work, we present an analytical model, and quantitatively analyze the giant CD of plasmonic splitting rectangle rings through theoretical means. The interplay of the electric and magnetic modes of the meta-structure is analyzed and considered to be responsible for the giant CD. The results show that

View Article Online
DOI: 10.1039/C5NR08527F

the circular current yielded by the splitting rectangle ring behaves like a magneton. The hybridization of the electric mode and the magnetic mode results in the mixing of the two modes. The analytical model, as well as the finite element method (FEM, COMSOL multiphysics) analysis, matches the CD quite well in a quantitative sense. Moreover, the splitting rectangle rings of different parameters are further investigated. An analysis of the chiral near-fields of the structures reveals potential applications for chiral molecule sensing.

Model

The structure investigated in this work is the well-known splitting rectangle ring shown in Figure 1, which has been much investigated in recent years.[27-29] We consider the gold splitting rectangle ring (optical constants from Johnson and Christy) located in the x-y plane and the incident light propagating in the y-z plane with θ representing the angle of **k** from the z axis and φ representing the angle from the x-axis. The length and width of the rectangular ring were set to the same value l, the thickness and the right asymmetric arm were set as h and a, respectively, and the gap was set as d, each of which are marked in Figure 1a and b. All calculations were performed by assuming that the structure is in a homogeneous surrounding medium with an effective refractive index of 1.1. The circular dichroism of the system was calculated as the difference in extinction under left- and right-handed circularly polarized light ($CD = \sigma_L - \sigma_R$). To satisfy the extrinsically chiral excitation criteria, the splitting gap cannot be located in the middle of the long side; thus, a = 20 nm. Oblique excitation with the wavevector **k** that is not in the plane is determined by the normal and symmetric axis of the structure, which will cause the CD effect. Here, when excited as shown in Figure 1b, an enormous CD can be obtained in the dipole peak, and it exhibits more than a 90% difference (Figure 1c and 1d). The huge CD in the dipole mode is seldom reported. As indicated, there is no optical activity under normal incidence (θ = 0°) (black line in Figure 1d) because there is reflection symmetry in the plane that is perpendicular to the propagation direction. When the incident angle is changed from θ = 45° to θ = -45°, the CD spectra are reversed. The θ is set to 45° in the following studies.

Hybridization of the modes and formation of the chiral response

To draw out the analytical model easily later, we first analyze the surface plasmon modes that are supported by the splitting rectangle ring under different excitation polarizations (the illumination direction is the same as it is in Figure 1b). Hybridization is a convenient way to understand the interaction of the structures.[30] Figure 2a shows the hybrid diagram of the rectangle ring under p-polarized light ($\vec{E}$ in the y-z plane). The left and right panels in Figure 2a are for the larger and smaller parts, respectively, and the middle panel is for the whole ring structure. From the surface charge distributions, one can easily determine that the four peaks of the whole ring are bonding modes and anti-bonding modes, in which peaks 1, 3 and 4 are bonding modes and peak 2 is an anti-bonding mode. For s-polarized light ($\vec{E}$ along x), the condition is a bit different (Figure 2b). Because of the retardation in the light-propagating direction, some modes that oscillate perpendicular to the x direction will appear

View Article Online
DOI: 10.1039/C5NR08527F

(peak 1', 2'', 3'') in the two individual parts. However, according to Figure 2b, one can still see that all the peaks are bonding modes. From the surface charge distributions in Figure 2a and 2b, it is easy to see that peaks 1 and 3 are dark modes, in which the current flows in a circle, acting as a magnetron (see supporting information Figure S1). Peaks 2 and 4 are the bright modes, and they act as electric dipoles and quadruples.

Because circularly polarized light can be decomposed into s and p-polarized light with a $\pi/2$ phase difference, we analyze the CPL situations by combining the results of s and p polarization excitations in Figure 2a and 2b, and in the following section, we will focus on the four primary peaks (which are marked in Figure 2c and 2d). Figure 2c shows the condition for left-handed circularly polarized light (LCP), with the middle panel showing LCP excitation and the left and right panels under linearly polarized p and s light. In Figure 2c, we can see that the four modes for LCP (i, ii, iii and iv) correspond to modes i', ii' and iv' for p-polarized light and i'', iii'' and iv'' for s polarized light. The surface charge distributions for p-polarized light are plotted in phase $-\pi/2$, and for s, it is 0, which is consistent with the incident light of LCP. For peak i, one can see that the surface charges for s and p light are in phase oscillation; thus, the superposition of the two modes will strengthen each other, making peak i stronger. Because peaks ii and iii originate only from p or s light, they are not weakened or strengthened during a ***direct view*** of this picture (the intensity change comes from the mixing of electric and magnetic modes, which will be analyzed later). For peak iv, the surface charge distributions indicate that iv' and iv'' are oscillating out of phase in the opposite direction; thus, this peak is weakened in LCP, and the effective oscillation is similar to a weak quadruple. Similarly, the condition for right-handed circularly polarized light (RCP) is shown in Figure 2d. The surface charge distributions for p-polarized light are plotted in phase $\pi/2$ and 0 for s, which is consistent with the incident light of RCP. Peak i is weakened and peak iv is strengthened, and peaks ii and iii are somehow non-weakened and non-strengthened.

The diagrams in Figure 2c and 2d explain the origination of the CD signals of the splitting rectangle ring structure from a direct point of view; however, the origin of CD for peak ii and peak iii is not yet clear. For a better understanding of the origin of the CD in the plasmonic structure, we propose an analytical model in the following section, and we examine this theory using the FEM model.

Mode mixing for coupled electric and magnetic dipoles

According to Figure 2c and 2d, we know that the dark modes (peak i and peak iv) oscillate in a circular way, which is equivalent to a magneton, and that the bright modes (peak ii and peak iii) are electric dipoles. Analogous to chiral molecules, when the electric dipole and magnetic dipole interact with one another in chiral plasmonic structures where the electric dipole, magnetic dipole and wave vector consist of a three-dimensional configuration that cannot overlap with its mirror form, regardless of its intrinsic or extrinsic chirality, there will be CD. For a symmetric configuration, even if there are strong magnetic modes, the electric dipole is always orthogonal to the magnetic dipole such that there is no CD. For a plasmonic meta-molecule with excited magnetic and electric dipole modes both, there is a mixed

View Article Online
DOI: 10.1039/C5NR08527F

electric-magnetic dipole polarizability of $G = G' + iG''$, causing electric dipole moment p_e and magnetic dipole moment p_m [22]

$$\widetilde{\boldsymbol{p_e}} = \tilde{\alpha}\widetilde{\boldsymbol{E}} - i\tilde{G}\widetilde{\boldsymbol{B}},\ \widetilde{\boldsymbol{p_m}} = \tilde{\chi}\widetilde{\boldsymbol{B}} - i\tilde{G}\widetilde{\boldsymbol{E}}, \text{(1)}$$

where $\alpha = \alpha' + i\alpha''$ is the electric polarizability and $\chi = \chi' + i\chi''$ is the magnetic susceptibility. $\boldsymbol{E}$ and $\boldsymbol{B}$ are the local fields at the meta-molecule.

The extinction of the meta-molecule is

$$A^{\pm} = \frac{\omega}{2} Im\left(\widetilde{\boldsymbol{E}}^* \cdot \widetilde{\boldsymbol{p_e}} + \widetilde{\boldsymbol{B}}^* \cdot \widetilde{\boldsymbol{p_m}}\right) = \frac{\omega}{2}\left(\alpha''\left|\widetilde{\boldsymbol{E}}\right|^2 + \chi''\left|\widetilde{\boldsymbol{B}}\right|^2\right) + G''^{\pm}\omega\, Im(\widetilde{\boldsymbol{E}}^{\pm *} \cdot \widetilde{\boldsymbol{B}}^{\pm}), \text{(2)}$$

$$\Delta A = G''^{+}C^{+} - G''^{-}C^{-}, \text{(3)}$$

where $C = -\frac{\varepsilon_0\omega}{2} Im(\boldsymbol{E}^* \cdot \boldsymbol{B})$ is the electromagnetic field chirality[22]. $C_{CPL} = \pm\frac{\varepsilon_0\omega}{2c}E_0^2$ is the optical chirality for a right (−) or left (+) circularly polarized plane wave with the electric field amplitude E_0. Here, we use $G''^{\pm}$ because the magnetic dipole is induced by plasmonic resonance, which is different for LCP and RCP, and for normal chiral molecules, the intrinsic electric and magnetic polarizability is fixed. By following Schellman and Govorov [31, 32] we obtain

$$G'' = -Im(\boldsymbol{p_e} \cdot (-i\boldsymbol{p_m})). \text{ (4)}$$

In keeping the above information in mind, we first investigated the system of coupled plasmonic electric and magnetic dipoles with the coupled-dipole approximation method (see Supporting Information for details)[33, 34]. The dipole moments of the two coupled dipoles can be expressed as[35, 36]

$$\boldsymbol{p_e} = \varepsilon_0\overleftrightarrow{\boldsymbol{\alpha_1}}\left(\boldsymbol{E_{1,in}} - Z_0k^2\overleftrightarrow{\boldsymbol{G_m}}(\boldsymbol{r_e}, \boldsymbol{r_m})\boldsymbol{p_m}\right), \text{ (5)}$$

$$\boldsymbol{p_m} = \overleftrightarrow{\boldsymbol{u_2}}\left(\boldsymbol{H_{2,in}} + ck^2\overleftrightarrow{\boldsymbol{G_m}}(\boldsymbol{r_m}, \boldsymbol{r_e})\boldsymbol{p_e}\right), \text{ (6)}$$

where $\overleftrightarrow{\boldsymbol{\alpha_1}}$ and $\overleftrightarrow{\boldsymbol{u_2}}$ are the polarizability tensors and $\overleftrightarrow{\boldsymbol{G_m}}(\boldsymbol{r_j}, \boldsymbol{r_k})$ is the electric dyadic Green's function. In solving this set of two equations, we can obtain the self-consistent forms of dipole moments

$$\boldsymbol{p_e} = \frac{\varepsilon_0\overleftrightarrow{\boldsymbol{\alpha_1}}\boldsymbol{E_{1,in}} - Z_0k^2\varepsilon_0\overleftrightarrow{\boldsymbol{\alpha_1}}\overleftrightarrow{\boldsymbol{G_m}}(\boldsymbol{r_m}, \boldsymbol{r_e})\overleftrightarrow{\boldsymbol{u_2}}\boldsymbol{H_{2,in}}}{\overleftrightarrow{\boldsymbol{I}} + \boldsymbol{c}Z_0k^4\varepsilon_0\overleftrightarrow{\boldsymbol{\alpha_1}}\overleftrightarrow{\boldsymbol{G_m}}(\boldsymbol{r_m}, \boldsymbol{r_e})\overleftrightarrow{\boldsymbol{u_2}}\overleftrightarrow{\boldsymbol{G_m}}(\boldsymbol{r_e}, \boldsymbol{r_m})}, \text{(7)}$$

$$\boldsymbol{p_m} = \frac{\overleftrightarrow{\boldsymbol{u_2}}\boldsymbol{E_{2,in}} + \boldsymbol{c}k^2\varepsilon_0\overleftrightarrow{\boldsymbol{u_2}}\overleftrightarrow{\boldsymbol{G_m}}(\boldsymbol{r_e}, \boldsymbol{r_m})\overleftrightarrow{\boldsymbol{\alpha_1}}\boldsymbol{E_{1,in}}}{\overleftrightarrow{\boldsymbol{I}} + \boldsymbol{c}Z_0k^4\varepsilon_0\overleftrightarrow{\boldsymbol{u_2}}\overleftrightarrow{\boldsymbol{G_m}}(\boldsymbol{r_e}, \boldsymbol{r_m})\overleftrightarrow{\boldsymbol{\alpha_1}}\overleftrightarrow{\boldsymbol{G_m}}(\boldsymbol{r_m}, \boldsymbol{r_e})}, \text{(8)}$$

where $\overleftrightarrow{\boldsymbol{I}}$ is the unit dyad. Then, the extinction of the system is

$$A^{\pm} = \frac{\omega}{2} Im(\boldsymbol{E}^* \cdot \boldsymbol{p_e} + \boldsymbol{B}^* \cdot \boldsymbol{p_m}). \text{ (9)}$$

View Article Online
DOI: 10.1039/C5NR08527F

Figure 3 shows the spectra of individual uncoupled dipoles and coupled dipoles under tilted LCP and RCP illuminations. The electric dipoles and magnetic dipoles are orthogonal in the incident plane, as shown in the Figure 3a inset. The polarizability of the electric dipoles $\overleftrightarrow{\boldsymbol{\alpha_1}}$ and the magnetic susceptibility of the magnetic $\overleftrightarrow{\boldsymbol{u_2}}$ are set on the basis of an ellipsoid particle, with the long axis along x for the electric dipole and along z for the magnetic dipole (see Figure 3a and supporting information). The blue and red curves in Figure 3a indicate individual electric and magnetic dipoles, respectively, which are resonant at different wavelengths. When they are coupled together, one can see that the hybrid electric mode exhibits blue shifts and that the magnetic mode has red shifts, as expected, because of the hybridization. There is a dip right at the individual magnetic resonant wavelength, which is known as Fano resonance. Not surprisingly, the coupled system shows the CD effect because of the mixed polarizability of the electric and magnetic dipoles, just like the chiral molecules. To obtain a clearer picture, the dipole extinction power of the individual dipoles for the coupled system is plotted in Figure 3b. One can see that even if there is only an electric (magnetic) moment for uncoupled dipoles, when they are coupled together, both the resonant peaks have mixed electric and magnetic moments. Thus, there are electric and magnetic component interactions in both electric and magnetic hybrid modes. Figure 3c shows the CD spectra for a direct LCP and RCP extinction difference (red curve) and for formulas 3 and 4 (blue curve). These spectra match very well with each other, as shown here. This finding indicates that the CD generation mechanism of the extrinsic plasmonic chiral structures is quantitatively determined and connected to the CD spectrum by the interaction and mixing of electric and magnetic excitations.

To verify the above mechanism, the plasmonic structure shown in Figure 1 is investigated in the same way as that of the analytical model, but with the electric and magnetic dipoles that were obtained from the numerical FEM results (Figure 4). Figure 4a shows the CD spectrum of an extinction difference for LCP and RCP. The electric and magnetic dipole moments are obtained with[37] [classic electromagnetic dynamics, Jackson]

$$\boldsymbol{p_e} = \int d^3r' \boldsymbol{r}' \rho(\boldsymbol{r}'), \quad (10)$$

$$\boldsymbol{p_m} = \frac{1}{2}\int d^3r' \ (\boldsymbol{r}' \times \boldsymbol{J}), \quad (11)$$

where $\rho(\boldsymbol{r}')$ is the charge density and $\boldsymbol{J}(\boldsymbol{r}')$ is the current density. The derived electric and magnetic dipole power are plotted in Figure 4b. Very similar to the hybrid condition in Figure 3, the electric and magnetic dipole resonances are mixed together, showing magnetic components at all resonant peaks. The magnetic dipole moment is much stronger in this hybrid structure because the split-ring resonators are able to tremendously enhance the total decay rate of the magnetic dipole emitters.[29] We should make it clear that the two peaks with higher energy represent multiple oscillations, which is not considered in our model and will thus be discussed later. With the derived electric and magnetic dipole moments, the CD spectrum can be calculated using formulas 3 and 4, as shown in Figure 4c. This spectrum is very similar to the curve in Figure 4a for the two lower energy modes. This finding confirms our analytical mechanism for Figure 3 quantitatively, which is a further step in explaining the extrinsic plasmonic chiral structures compared with the previous ones. However, this approach only works for

View Article Online
DOI: 10.1039/C5NR08527F

dipole modes. For multiple modes, there is more than one equivalent magnetic dipole that is oscillating out of phase; however, with the delayed interaction with the electric modes, the whole effect is an interference superposition[21]. While the hybrid model proposed here does not account for the multiple and phase delays, so there is a very large deviation for multiple modes (the left part of the black dot-dashed line in Figure 4).

Because the electric dipole emitter and the induced magnetic dipole emitter have phase differences depending on the wavelength, they will cause a Fano-type line shape, as proven in other works.[21] Because both the CD effect and Fano-type spectra are related to the electric and magnetic dipole (or dark mode) interactions, once there is a CD effect in the plasmonic structures, there is a Fano-type line shape in the spectrum.

Parameter-dependent chirality

To investigate the CD of this structure further, the dependence of the CD effect on several parameters of the system is studied as well, as shown in Figure 5. Figure 5a and 5b show the extinction and CD spectra of the splitting rectangle rings that were excited by CPL light when right asymmetric arm a varies from 40 nm to 0 nm, and the gap and the total length of the rectangle ring are kept constant (as shown in Figure 1a; d = 20 nm, l = 200 nm, h = 30 nm, and w=40 nm). When the right arm becomes shorter and the left one becomes longer, all the hybrid modes experience a red shift, except the ii modes (which are dominated by the shorter arm, as shown in Figure 2), and the intensity increases (Figure 5a and 5b). As the left arm increases, the total magnetic mode becomes stronger, increasing the CD of the structure. The asymmetric Fano profile simultaneously becomes more distinctive and thus induces an increase in the CD response (Figure 5b).

The thickness of the system has a significant effect on the CD response. Splitting rectangle rings with thicknesses of 20 nm, 40 nm, and 60 nm were studied, as shown in Figure 5c and 5d, with the other parameters remaining unchanged (a = 20 nm, d = 20 nm, l = 200 nm, and w = 40 nm). From Figure 5c, it is apparent that all the resonant peaks exhibit a blue shift, and the extinction cross section of peak i increases under LCP excitation but decreases under RCP excitation. When the thickness changes to 60 nm, the structure exhibits total left-handedness. This finding is explained by the fact that when the cross section of the bar increases, the induced current and dipole moment will increase; thus, the corresponding CD response is markedly enhanced as the thickness increases, with a stronger interplay of the electric and magnetic dipoles (Figure 5d). This stronger and stronger interaction causes a total CPL selection in the lowest mode, which is seldom observed in plasmonic chirality.

Chiral near-field properties and sensing

View Article Online
DOI: 10.1039/C5NR08527F

One of the most important issues related to plasmonic chiral structures is the chiral near-field enhancement in chiral molecule detection and sensing. For chiral molecules, the CD signal follows the same relation as that in formula 3, but with fixed mixed electric and magnetic polarizability G''[5]

$$\Delta A = G''(C^+ - C^-) = 2G''|C_{CPL}|. \quad (12)$$

For plasmonic structures that enhance chiral molecule detection,[25] the integration of the local chiral field where the molecules are adsorbed determines the CD signal. The enhancement factor for the chirality of the field $\hat{C} = C/|C_{CPL}|$ is considered in the following. The whole chiral field enhancement is the volume-averaged chiral spectra where the molecule is located, and it is calculated using [26]$\langle \hat{C} \rangle = \frac{1}{V}\int_V \hat{C} \cdot dV$.

We first investigated the chiral near-field distributions of the same structure as that in Figure 1 (Figure 6). Figure 6a shows the electric field enhancement at the four resonant peaks under RCP and LCP excitation. It is not surprising that the fields in the splitting gaps are clearly enhanced. Note that the field enhancement in the two gaps has different selectivity for the handedness of the exciting light and for the resonant modes. For instance, the electric field in the upper gap is stronger at 1610 nm, with 700 nm for RCP and 1080 nm for LCP; the electric field in the lower gap is stronger at 1080 nm for RCP. This finding may have potential applications in selective photo-catalysis. Moreover, it is notable that the chiral field in the gaps is also clearly selective for LCP and RCP, as shown in Figure 6b. The upper gap enhances the RCP chiral field at 1610 nm, 840 nm, and the LCP chiral field at 1080 nm, 840 nm. The lower gap enhances the RCP chiral field at 1080 nm, and the LCP chiral field does the same at 1610 nm. If one focuses on one resonant peak, e.g., the 1610 nm peak, the RCP light will excite a strong chiral field in the upper gap, and the LCP light will excite a stronger chiral field in the lower gap. The case is reversed for the 1080 nm peak. The selective switching enhancement of the chiral field for CPL is very useful in chiral molecule sensing and catalysis. In most traditional plasmonic structures for chiral field enhancement, the target gaps have an enhancement effect for both LCP and RCP, but here, at the resonant peak of 1610 nm, the upper gap keeps the C^- field and the lower gap keeps the C^+ field; at the resonant peak of 1080 nm, the upper gap keeps the C^+ field and the lower gap keeps the C^- field.

In real applications, one usually hopes that the left-handed chiral molecules are enhanced by the C^+ field and that the right-handed chiral molecules are enhanced by the C^- field. Here, this selective enhancement of chiral fields may be useful for catalyzing chiral chemical reactions or simultaneous detection.

To view these selective chiral fields directly and clearly, the volume-averaged chiral field enhancement $\langle \hat{C} \rangle$ spectra in the upper gap (Vol 1) and lower gap (Vol 2) are plotted in Figure 7. From the spectra, one can clearly see that for the 1610 nm mode, the chiral field in Vol 1 is always negative, and it is always positive in Vol 2; for the 1080 nm mode, the opposite is true. The larger difference for the 1610 nm mode is more important and applicable in practice.

Conclusion and discussion

View Article Online
DOI: 10.1039/C5NR08527F

In this work, the generation mechanism of extrinsic plasmonic chirality is quantitatively presented using an analytical model of coupled plasmonic electric and magnetic dipoles. The strong interplay of electric and induced magnetic dipoles will cause a mixed electric and magnetic polarizability, which is responsible for the CD of the meta-molecule from LCP and RCP light. The model is verified using the numerical FEM results of splitting rectangle rings. The results show that the circular current yielded by the splitting rectangle rings behaves like a magneton. The hybridization of the electric mode and the magnetic mode results in a mixing of the two modes, coincident with the above analytical model. The parameter-dependent CD response of the splitting rectangle rings is also investigated. The analysis of the chiral near-field of the structure shows potential applications for chiral molecule sensing.

According to the molecular optical activity theory, the quantification of the mechanism underlying the plasmonic CD effect by both analytical and numerical models is expected to be applicable to all the plasmonic extrinsic chiral structures, which will be a continuous issue in the future. Expanding the model to higher-order modes is necessary and requires more work because higher-order modes may exhibit stronger CD [21].

Methods

FEM simulation: All full wave numerical simulations were performed by using the finite element method (FEM, commercial software package, Comsol Multiphysics 4.3a). The Au splitting rectangle ring was placed in a homogeneous surrounding medium with an effective refractive index of 1.1. Non-uniform meshes were used to format the object. The largest mesh was set to less than $\lambda / 6$. A perfect matched layer (PML) was used to minimize the scattering from the outer boundary. The nano-ring was placed in the x-y plane. The incident light was set to 1 V/m and propagated in the y-z plane off the z axis. The total scattering cross sections were obtained by integrating the scattered power flux over an enclosed surface outside the nano-ring, and the absorption cross sections were determined by integrating the Ohmic heating within the nano-ring. The circular dichroism of the system was calculated as the difference in extinction under left and right-handed circularly polarized light ($CD = \sigma_L - \sigma_R$). The super chiral field was plotted with $\hat{C} = C/|C_{CPL}|$, where C is defined as $C = -\frac{\varepsilon_0 \omega}{2} Im(\boldsymbol{E}^* \cdot \boldsymbol{B})$ and $C_{CPL} = \pm \frac{\varepsilon_0 \omega}{2c} E_0^2$. The volume-averaged chiral spectra were obtained using $\langle \hat{C} \rangle = \frac{1}{V} \int_V \hat{C} \cdot dV$

The coupled dipole approximation method: It is too long to include here; please view the supporting information for details.

Acknowledgments

This work was supported by the National Natural Science Foundation of China (11204390), the Natural Science Foundation Project of CQ CSTC (2014jcyjA40002), the Science and Technology Project of CQ Commission of Education (KJ1500636) and the Special Fund for Agro-scientific Research in the Public Interest (201303045).

Author contributions

View Article Online
DOI: 10.1039/C5NR08527F

Y. Fang launched and supervised the project. L. Hu conducted the FEM simulations, and X. Tian wrote the expressions of the electric and magnetic dipoles for FEM. Y. Fang proposed the analytical dipole model and wrote the Matlab codes. Y. Fang and X. Tian discussed the coupling mechanism of the dipoles. Y. Fang analyzed all the data and wrote the paper. All of the authors contributed useful suggestions and revised the paper.

Competing financial interests: The authors declare no competing financial interests.

Supporting Information is available for near-field distributions in the magnetic field of the splitting rectangle ring and the coupled electric and magnetic dipoles methods.

References:

1. L. D. Barron, *Molecular Light Scattering and Optical Activity*, Cambridge University Press, Cambridge, 2nd edn., 2004.
2. A. Kuzyk, R. Schreiber, Z. Y. Fan, G. Pardatscher, E. M. Roller, A. Hogele, F. C. Simmel, A. O. Govorov and T. Liedl, *Nature*, 2012, **483**, 311-314.
3. S. A. Maier, *Plasmonics: fundamentals and applications*, Springer, United Kingdom, 2007.
4. V. K. Valev, J. J. Baumberg, C. Sibilia and T. Verbiest, *Adv Mater*, 2013, **25**, 2517-2534.
5. A. Garcia-Etxarri and J. A. Dionne, *Phys Rev B*, 2013, **87**, 235409.
6. H. Zhang and A. O. Govorov, *Phys Rev B*, 2013, **87**, 075410.
7. M. Kuwata-Gonokami, N. Saito, Y. Ino, M. Kauranen, K. Jefimovs, T. Vallius, J. Turunen and Y. Svirko, *Phys Rev Lett*, 2005, **95**, 227401.
8. C. Gautier and T. Burgi, *Chemphyschem*, 2009, **10**, 483-492.
9. Z. Y. Fan and A. O. Govorov, *Nano Lett*, 2012, **12**, 3283-3289.
10. S. Droulias and V. Yannopapas, *J Phys Chem C*, 2013, **117**, 1130-1135.
11. W. S. Gao, C. Y. Ng, H. M. Leung, Y. H. Li, H. Chen and W. Y. Tam, *J Opt Soc Am B*, 2012, **29**, 3021-3026.
12. A. S. Schwanecke, A. Krasavin, D. M. Bagnall, A. Potts, A. V. Zayats and N. I. Zheludev, *Phys Rev Lett*, 2003, **91**, 247404
13. R. Schreiber, N. Luong, Z. Y. Fan, A. Kuzyk, P. C. Nickels, T. Zhang, D. M. Smith, B. Yurke, W. Kuang, A. O. Govorov and T. Liedl, *Nat Commun*, 2013, **4**, 2948.
14. P. Kuhler, E. M. Roller, R. Schreiber, T. Liedl, T. Lohmuller and J. Feldmann, *Nano Lett*, 2014, **14**, 2914-2919.
15. M. Schafering, X. H. Yin, N. Engheta and H. Giessen, *Acs Photonics*, 2014, **1**, 530-537.
16. M. Esposito, V. Tasco, F. Todisco, M. Cuscuna, A. Benedetti, D. Sanvitto and A. Passaseo, *Nat Commun*, 2015, **6**, 6484.
17. M. Esposito, V. Tasco, F. Todisco, A. Benedetti, I. Tarantini, M. Cuscuna, L. Dominici, M. De Giorgi and A. Passaseo, *Nanoscale*, 2015, **7**, 18081-18088.
18. E. Plum, V. A. Fedotov and N. I. Zheludev, *Appl Phys Lett*, 2008, **93**, 191911.
19. E. Plum, X. X. Liu, V. A. Fedotov, Y. Chen, D. P. Tsai and N. I. Zheludev, *Phys Rev Lett*, 2009, **102**, 113902.
20. T. Cao, C. W. Wei, L. B. Mao and Y. Li, *Sci Rep*, 2014, **4**, 7442.
21. X. R. Tian, Y. R. Fang and B. L. Zhang, *Acs Photonics*, 2014, **1**, 1156-1164.
22. Y. Q. Tang and A. E. Cohen, *Phys Rev Lett*, 2010, **104**, 163901.
23. D. M. Lipkin, *J Math Phys*, 1964, **5**, 696.
24. E. Plum, V. A. Fedotov and N. I. Zheludev, *J Opt a-Pure Appl Op*, 2009, **11**, 074009.
25. E. Hendry, T. Carpy, J. Johnston, M. Popland, R. V. Mikhaylovskiy, A. J. Lapthorn, S. M. Kelly, L. D. Barron, N. Gadegaard and M. Kadodwala, *Nat Nanotechnol*, 2010, **5**, 783-787.

View Article Online
DOI: 10.1039/C5NR08527F

26.R. Ogier, Y. R. Fang, M. Svedendahl, P. Johansson and M. Kall, *Acs Photonics*, 2014, **1**, 1074-1081.
27.T. D. Corrigan, P. W. Kolb, A. B. Sushkov, H. D. Drew, D. C. Schmadel and R. J. Phaneuf, *Opt Express*, 2008, **16**, 19850-19864.
28.R. L. Chern, *Phys Rev B*, 2008, **78**, 085116
29.S. M. Hein and H. Giessen, *Phys Rev Lett*, 2013, **111**, 026803.
30.E. Prodan, C. Radloff, N. J. Halas and P. Nordlander, *Science*, 2003, **302**, 419-422.
31.J. A. Schellman, *Chem Rev*, 1975, **75**, 323-331.
32.A. O. Govorov and Z. Y. Fan, *Chemphyschem*, 2012, **13**, 2551-2560.
33.P. C. Chaumet, A. Sentenac and A. Rahmani, *Phys Rev E*, 2004, **70**, 036606
34.P. C. Chaumet, K. Belkebir and A. Rahmani, *Opt Express*, 2008, **16**, 20157-20165.
35.G. W. Mulholland, C. F. Bohren and K. A. Fuller, *Langmuir*, 1994, **10**, 2533-2546.
36.S. N. Sheikholeslami, A. Garcia-Etxarri and J. A. Dionne, *Nano Lett*, 2011, **11**, 3927-3934.
37.J. D. Jackson, *Classical Electrodynamics*, Wiley, U.S.A, 3nd edn., 1998.

Figure captions

Figure 1 | Structures investigated and the chiral spectra. (a-b) Schematics of a splitting nano-ring, as seen from different views, with labeled structural parameters. The nano-ring is located in the x-y plane, and (b) is the excitation case chosen for this paper, with the y-axis along the connecting line of the two gaps. (c) Extinction spectra of the nano-ring (l = 200 nm, w = 40 nm, w = 20 nm, h = 30 nm, a = 20 nm) under LCP and RCP excitation (θ = 45°). (d) CD spectra of the nano-ring, as illuminated with different incident angles (θ = 45° (red), θ = 0° (black), θ = -45° (blue)).

Figure 2| Hybridization diagrams and mixed electric and magnetic modes. (a, b) Hybrid diagram of the structure with the same parameters as noted in Figure 1 under (a) p-polarized light excitation and (b) s-polarized light excitation. (c, d) Modes analysis under LCP (c) and RCP (d) excitation, with mixing p and s polarized light. The insets are surface charge distributions.

Figure 3 | Mode mixing for coupled electric and magnetic dipoles. Coupled dipole approximation calculations for a coupled electric dipole (ellipsoid a = 120 nm, b = c = 23 nm) and a magnetic plasmonic dipole (ellipsoid a = b = 4.5 nm, c = 30 nm) with a 60 nm separation in y direction. (a) Extinction spectra for uncoupled electric and magnetic plasmonic dipoles as well as coupled electric and magnetic plasmonic dipoles under CPL illumination. (b) The dipole power of the individual coupled electric and

View Article Online
DOI: 10.1039/C5NR08527F

magnetic plasmonic dipoles in (a). (c) Extinction difference (CD) of the coupled system (red curve) and the CD calculated from formulas 3 and 4 with imaginary part of the mixed electric and magnetic polarizability for the coupled system.

Figure 4 | Mode mixing for coupled electric and magnetic dipoles in FEM simulations. Coupled electric and magnetic dipole analysis for the splitting rectangle ring as shown in Figure 1. (a) The extinction difference (CD) of the structure. (b) The electric and magnetic dipole power yielded by the structure under CPL illumination. (c) The imaginary part of the mixed electric and magnetic polarizability of the structure under CPL illumination.

Figure 5 | Parameter-dependent CD effect. Extinction spectra of (a) the splitting rectangle ring with different asymmetric arms a and (c) the splitting rectangle ring with different thicknesses h. For a better perspective, every spectrum in this section has an offset of $10*10^{-14}$ m^2 compared with the one below it. (b, d) The CD spectra of the above splitting rectangle rings. Solid lines in the upper row represent LCP, and the dashed lines are for RCP.

Figure 6 | Enhancement distributions of field intensity and chirality. (a) The electric field enhancement and (b) chiral field enhancement of the structure in Figure 1 at the four resonant peaks under RCP and LCP illumination. The slices are cut in the middle of the thickness.

Figure 7 | Volume-averaged chiral field enhancement under LCP (a) and RCP (b) illumination.

View Article Online
DOI: 10.1039/C5NR08527F

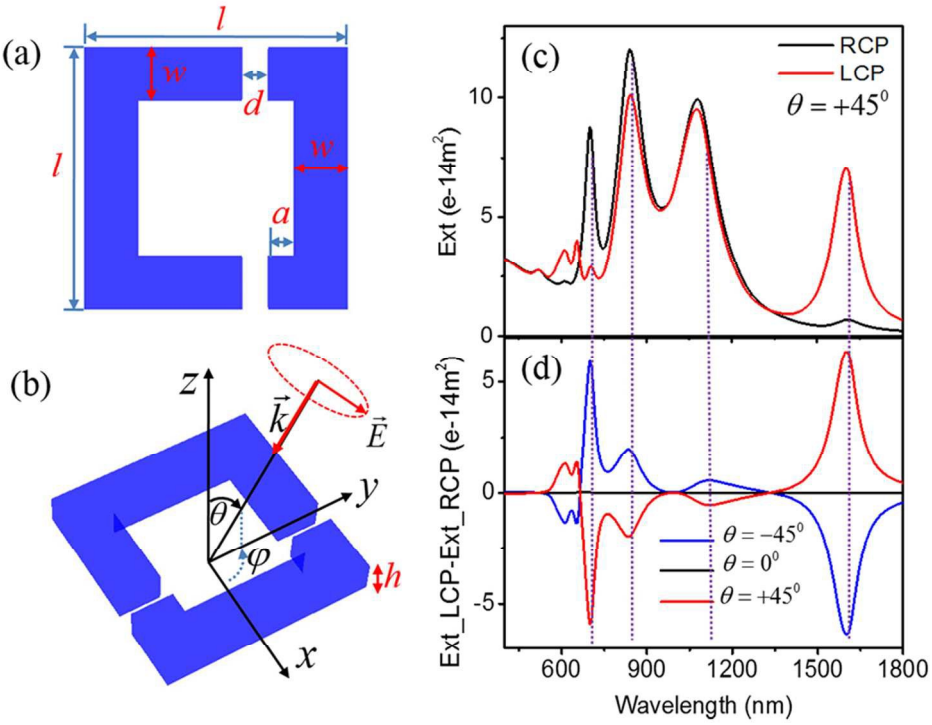

85x65mm (300 x 300 DPI)

View Article Online
DOI: 10.1039/C5NR08527F

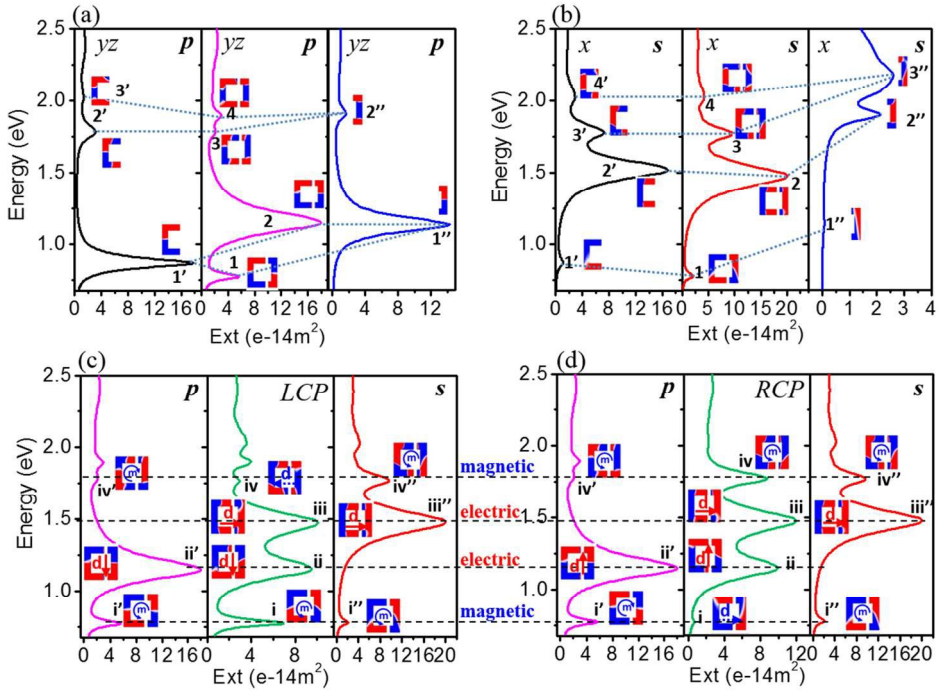

160x113mm (300 x 300 DPI)

View Article Online
DOI: 10.1039/C5NR08527F

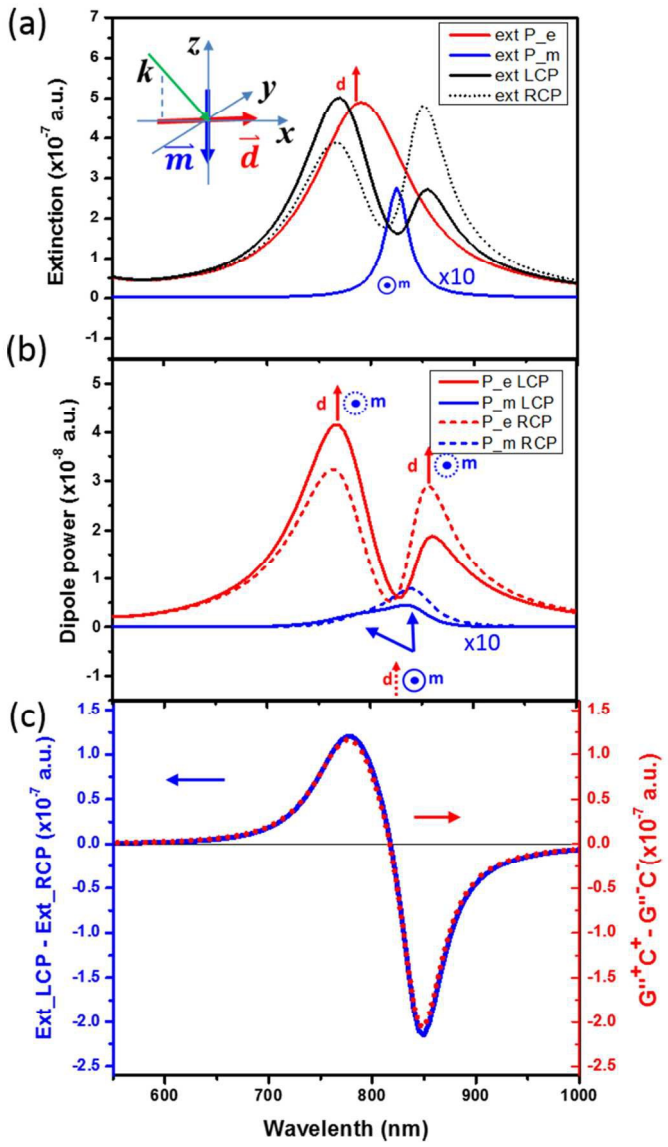

76x131mm (300 x 300 DPI)

View Article Online
DOI: 10.1039/C5NR08527F

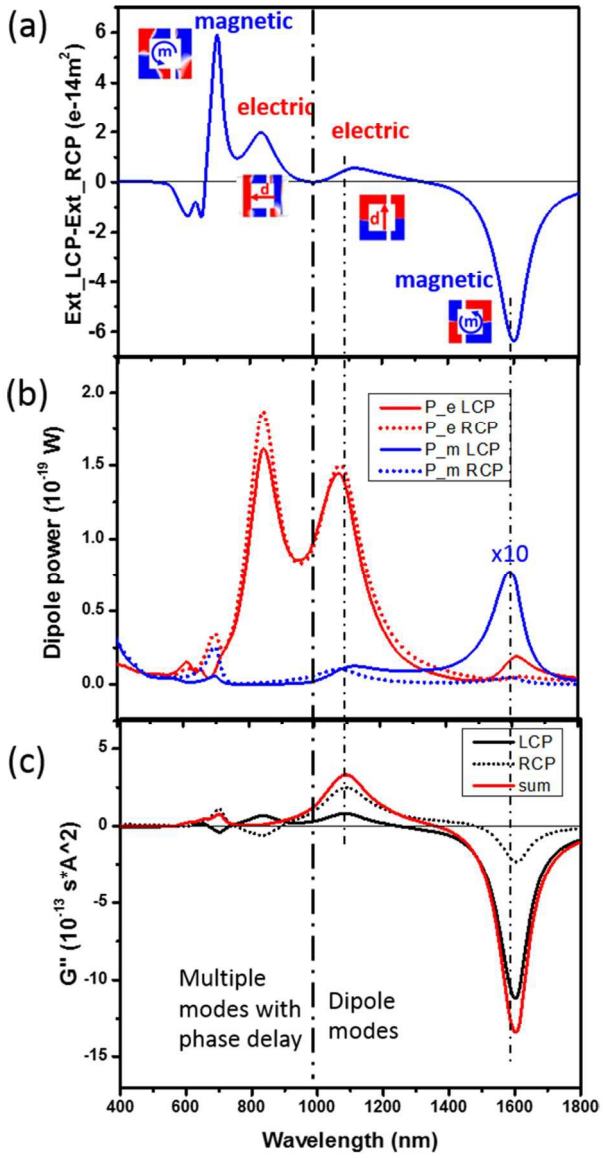

76x131mm (300 x 300 DPI)

View Article Online
DOI: 10.1039/C5NR08527F

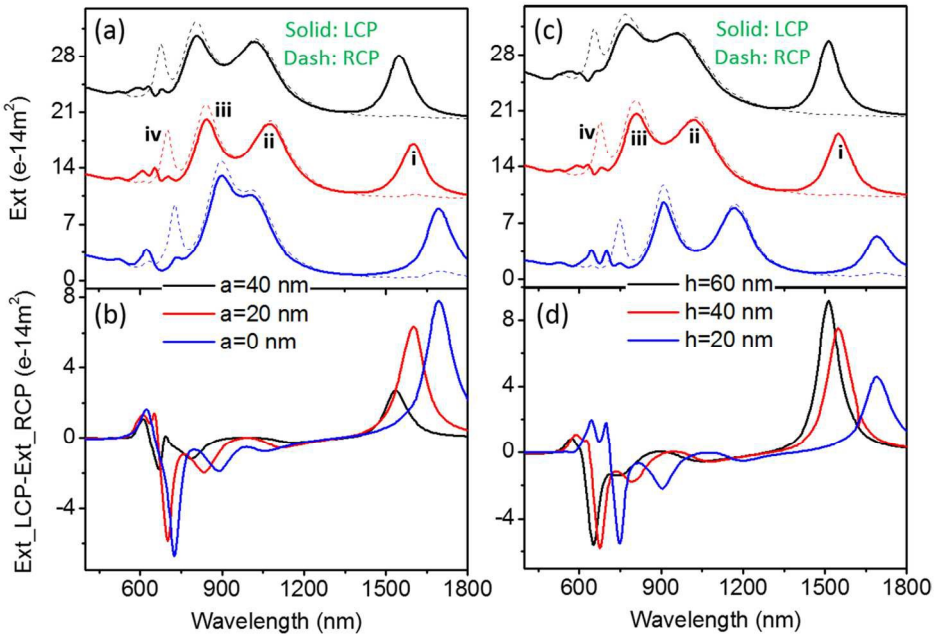

129x87mm (300 x 300 DPI)

View Article Online
DOI: 10.1039/C5NR08527F

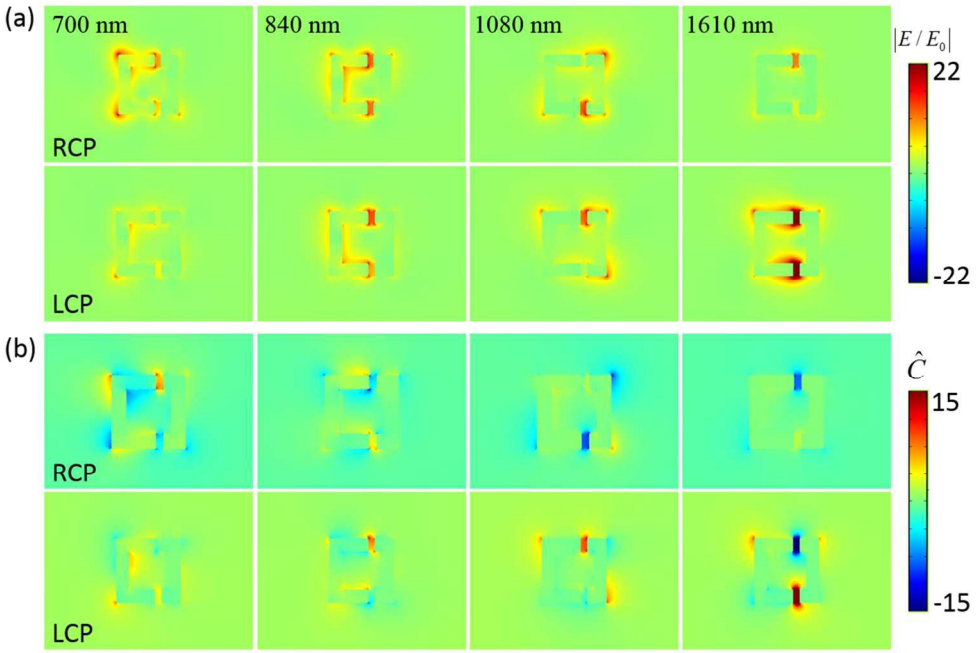

140x94mm (300 x 300 DPI)

View Article Online
DOI: 10.1039/C5NR08527F

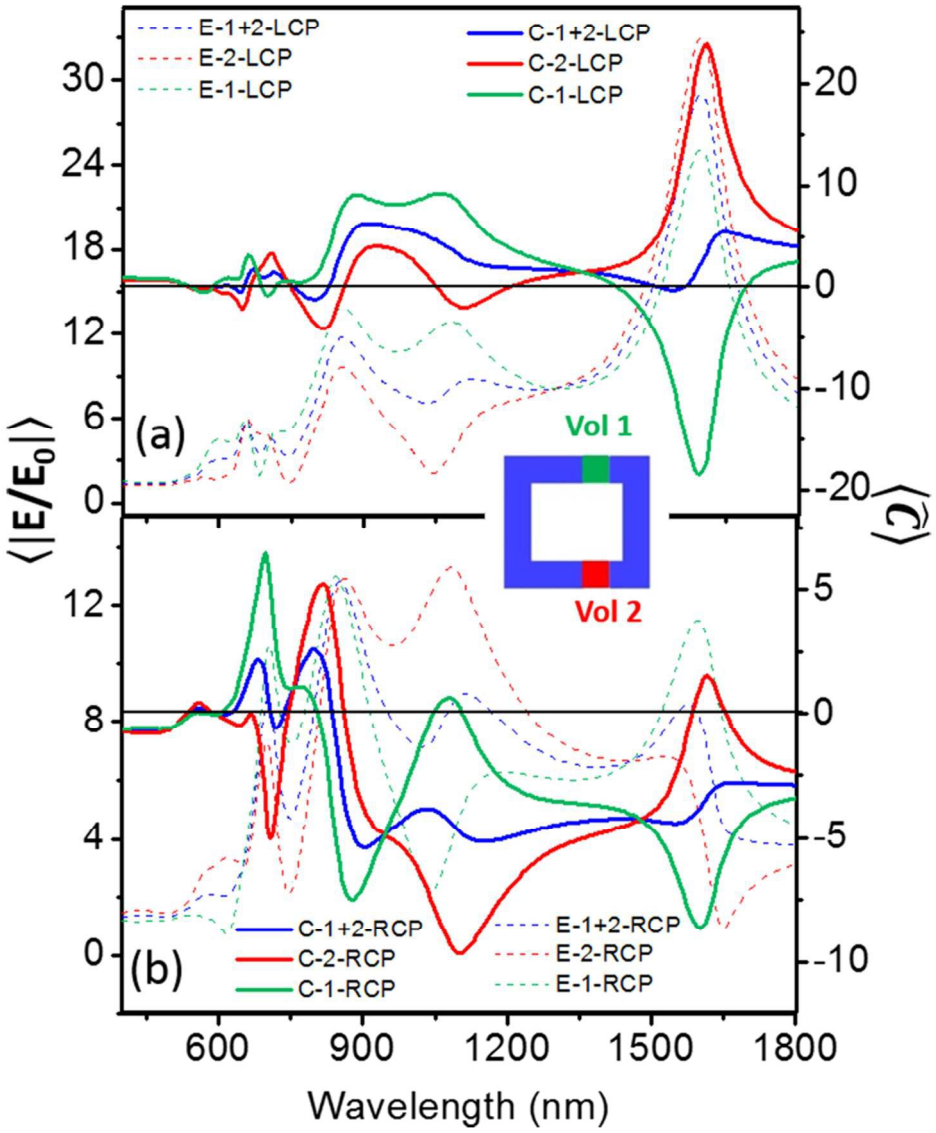

85x101mm (300 x 300 DPI)